HIGH SCHOOL EDITION
Journal of Student Research
Volume 13 Issue 4 (2024)

A Novel First Response, Search and Rescue (FRSR) System in Case of Disasters

Aias Tatsis

Pythagorian Gel of Samos, Greece

ABSTRACT

In this study, we introduce and rigorously test a novel First Response for Search and Rescue (FRSR) system, specifically designed for initial entry into natural or industrial disaster sites. The primary function of the FRSR is to provide immediate information to rescue teams regarding prevailing conditions within the affected area. The system's lightweight and compact design facilitates deployment by manual hurling or aerial means, while a safe landing system ensures controlled descents. Equipped with an all-terrain drive system, the FRSR can autonomously navigate and explore the area of interest. On-site capabilities include the transmission of infrared images and the measurement and transmission of vital environmental data, such as the Air Quality Index (AQI), the presence of hazardous gases, concentrations of Volatile Organic Compounds (VOCs), radiation levels, temperature, humidity, atmospheric pressure, and geographical coordinates. The data are transmitted wirelessly through an autonomous transmission system to a base station, located up to 2 km away from the disaster site, enabling rapid assessment and informed decision-making in critical rescue operations. During testing, the FRSR system exhibited highly accurate results, with consistent performance and no interruptions, demonstrating its potential as a reliable tool in disaster response scenarios.

Introduction

Natural disasters and industrial accidents can cause dangerous conditions for bystanders and rescuers. Most of the time the conditions prevailing at the disaster site are often undetermined [1,2,3] a wide range of possible conditions, making estimates practically impossible. The unclear circumstances cause delays in the intervention of rescuers, which is critical to the rescue success. Rescuers operate in an environment where they do not know the situation and need to take time to consider all possible cases, thus delaying the intervention. Of course, there are also cases where rescuers lose their lives operating in difficult and unknown conditions [1,2].

These observations underscore the urgent need for more predictive and adaptive systems to better understand and navigate disaster scenarios. Advancements in technology, such as artificial intelligence (AI), remote sensing, and Unmanned Aerial Vehicles (UAVs), provide promising avenues to facilitate the rapid assessment of disaster-stricken areas [4,5]. AI-powered models, for instance, can process data from various sources, such as weather conditions, seismic readings, and past disaster patterns, to provide timely and accurate estimates of prevailing conditions [6]. Similarly, UAVs equipped with high-resolution cameras and advanced sensors can offer real-time, aerial views of the disaster site, aiding the decision-making process [7]. These technologies, while not infallible, could drastically reduce the uncertainty facing first responders, increase their safety, and decrease response times. However, implementing these technologies also presents new challenges that must be addressed, such as the integration of disparate data sources, the real-time analysis of large data volumes, and the need for reliable communication infrastructure in the disaster area [8,9].

Related Work

Robotic systems have been proposed and used for intervention in disaster sites and have proven their usefulness in cases of disasters [2,4,7]. The systems proposed in the scientific literature can be divided into three major categories: autonomous systems with arms and cargo carrying capabilities, aerial autonomous and semi-autonomous UAV systems and autonomous systems of special conditions.

Autonomous systems with arms and cargo carrying capabilities [7], which have small potential to explore the area, as the rescuer must be close by, because the system cannot be deployed from a distance.

Promising systems in terms of capabilities are the aerial autonomous and semi-autonomous UAV systems that can approach the disaster site from above and record the prevailing conditions [4,5,6]. However, they require a specially trained operator, as they are costly and are at risk of crashing, which limits their ability to approach the disaster site. The proposed First Response, Search and Rescue (FRSR) system, with its lightweight of less than 300 grams, can be transported to the area of interest by a UAV and then launched at the specific spot.

There are also several autonomous systems of special conditions developed for intervention in specific areas or in special types of accidents, such as nuclear or chemical plants or to address terrorist acts. These systems cannot be used on different kind of disasters, except for the specific purpose for which they were built. Taking advantage of the latest technological developments, the FRSR system was created, which has small dimensions and weight, but also low construction costs. This allows all rescuers to have the FRSR with them and see on a computer or a mobile device the conditions prevailing in the area under investigation. In addition, the FRSR measures all possible forms of chemical, biological and radioactive hazards, as well as temperature and atmospheric pressure and can fall from a great height and move autonomously.

The author is not aware of an autonomous first response system that measures and transmits long-distance measurements of chemical, biological, or radioactive and atmospheric conditions. Most of the time, autonomous systems are bulky and cannot intervene in small spaces. In addition, they are usually costly and not all rescue teams can afford them or require special handling skills.

Another advantage of the FRSR is its specialized drive system, which ensures unhindered movement across any terrain. The mission can investigate conditions at sites of natural disasters or industrial accidents.

Methodology/Design & Development

Description of FRSR

The FRSR consists of two main systems, the Rover Unit (RU) and the Base Station (BS). The BS will be connected to the RU to receive data, store it and then process it. The RU consists of sensors, a central unit and a radio unit, which will be located in a common housing, with dimensions 115 mm long, 65 mm wide, and 40 mm high. At the top of the FRSR RU there will be communication and geolocation calculation antennas and a landing device (parachute).

The RU can be released from a height, its descent will be decelerated using a parachute, so that it descends at a speed of less than 7m/s. Or it can be launched by the rescuers to the place of interest and land again using a parachute. During descent, the data collected by the sensors will be recorded and sent to the BS.

The FRSR's RU has a post-landing powertrain to explore the surrounding area or head to a point of interest. Also, during landing, a system is put into operation to release the parachute from the body of the structure, so that it can move smoothly afterwards.

After landing, the area is explored with the RU propulsion system, and data gathered from the exploration area will continue to be sent to the BS. An important role of the thermal camera that can detect hot spots in space such as people or animals that may not be visible by visual observation. The Rover has autonomy of movement and data transmission for more than 1 hour and 30 minutes.

Mission

The mission is considered the exploration of the disaster area after the RU is released from a high altitude, over 200 m, into the disaster site. During the mission, the RU, records on a storage medium (SD memory card) and transmits to the base station the images of the thermal camera, ionizing radiation measurements and sensor values listed in Table 1. The BS will receive and store all the data.

Table 1. Measurements

Sensor	**Name**	**Unit**
AQI	Air Quality Index	0-(>350)
GAS	Pollution Indicator	0-100%
VOC	Organic Particles	ppm
CO_2	Carbon Dioxide	ppm
Hygrometer	Humidity	0-100%
Thermometer	Temperature	^oC
γ-radiation	Ionized Radiation	mSv
Pressure	Barometric Pressure	bar
Accelerometer	Acceleration	m/s^2

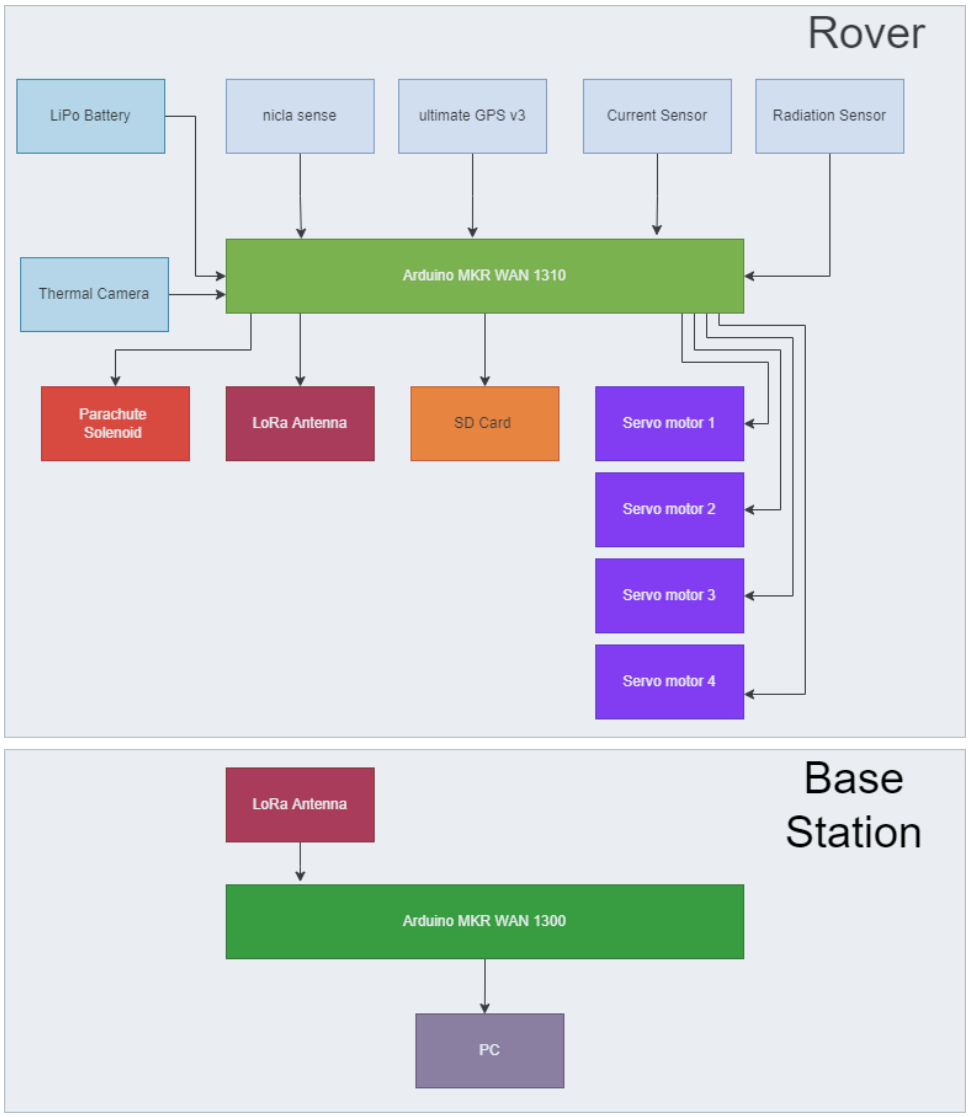

Figure 1. FRSR block diagram

After landing, the system will move around the drop point, continuing to transmit sensor readings. The direction of motion is generated by a stochastic algorithm to investigate the space in the best possible way. In addition, it is possible to move, if necessary, to a specific point of interest which can be controlled remotely by the rescuers.

AQI and Gas Sensors

The value of the AQI index and the GAS Sensor is derived from the Nicla Sense ME sensor, according to the specifications issued by the German Federal Environmental Agency [8].

Table 2. AQI and GAS Specifications

Air Quality Index			
AQI Index	**Air Quality**	**Impact (Long-term exposure)**	**Suggested action**
0-50	Excellent	Pure air, best for well-being	

51-100	Good	No limitation well-being	No measures needed
101-150	Lightly Polluted	Reduction of well-being possible	Ventilation Suggested
151-200	Moderately Polluted	More significand irritation possible	Increase ventilation with clean air
201-250	Heavily Polluted	Exposition might lead to effects like headache depending on type of VOCs	Optimize ventilation
251-350	Heavily Polluted	More severe health issue possible if harmful VOC present	Contamination should be identified if levels is reached even w/o presence of people; maximize ventilation & reduce attendance
>351	Extremely Polluted	Headaches, additional neurotoxic effects possible	Contamination needs to be identified; avoid presence in room and maximize ventilation
GAS Indication Specifications			
Molar Fraction	**Compound**	**Tolerance**	**Accuracy**
5 ppm	Ethane	20%	5%
10 ppm	Isoprene/2-methyl1,3Butadiene	20%	5%
10 ppm	Ethanol	20%	5%
50 ppm	Acetone	20%	5%
15 ppm	Carbon Monoxide	20%	5%

Engineering Design

The mechanical construction of RU is ~~3d~~ 3D printed, made of Nylon Polyamide Carbon Fiber (PA CF) filament with low weight, high mechanical properties, 105 MPa tensile strength, 170 MPa bending strength and resistant to temperatures up to 250 °C. PA CF (Polyamide Carbon Fiber) is well known for its electrical properties as it is a composite material with good electrical conductivity. This characteristic must be taken into account to prevent short circuits and to avoid potential communication issues, as it can act as a Faraday cage. On the other hand, it also provides insulation from electromagnetic interference, thereby protecting electronic circuits.

The case consists of a parallelepiped tube hat is closed permanently at the bottom, while on the other side (upper part) and a removable lid with a special locking socket. The upper part has an additional swivel-type rotating hook for attaching the parachute and a parachute release mechanism. For ground movement the RU has four arms driven by servo motors. The arms are designed so that the RU structure can move despite its small size on the ground with obstacles such as stones and sand.

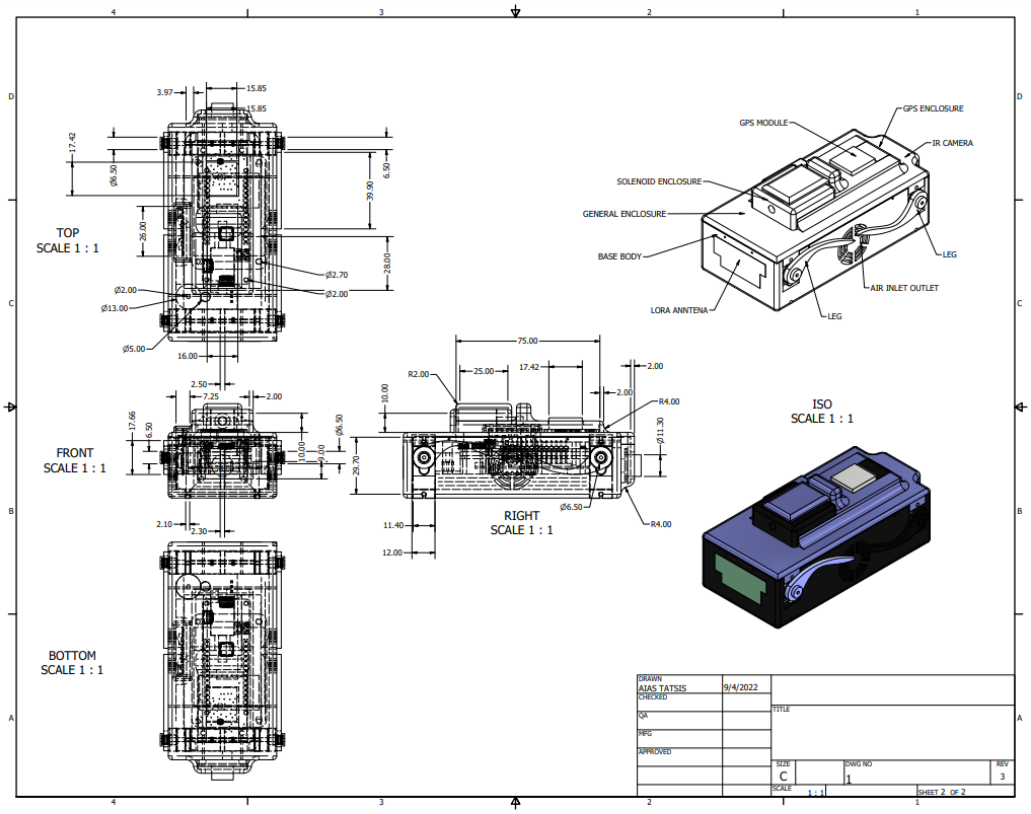

Figure 2. Mechanical Drawing

The RU internally has brackets for fastening the electronic components and ventilation holes to cool the electronic components and provide airflow to the sensors.

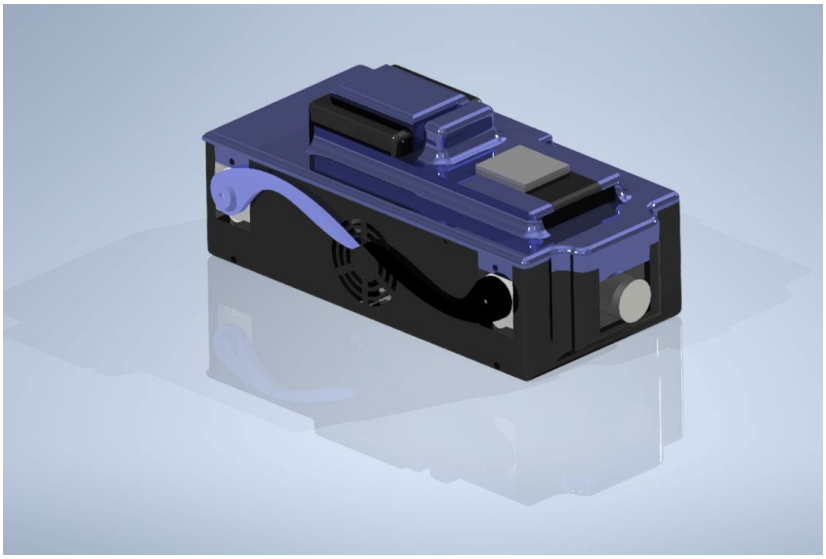

Figure 3. Three-dimensional model of assembled RU

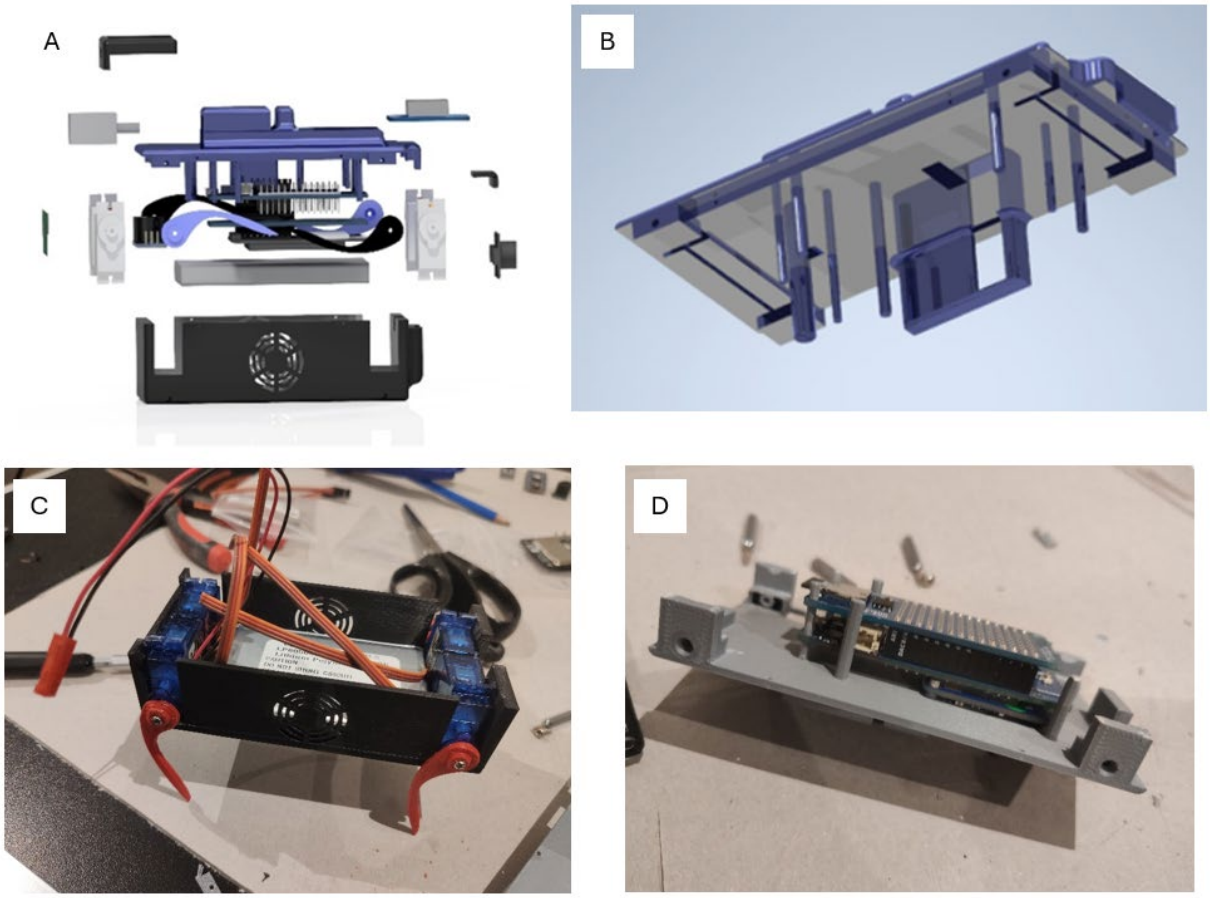

Figure 4. A. RU 3D model in explode view B. Rover cup 3D model, C. RU base assembly with motors and battery, D. RU cup assembly with the boards

Electrical Diagram

The electrical design of RU includes the sensors, the Arduino MKR WAN 1310 microcontroller, the data transfer and power supply connections as follows:

- The motors receive power from the Arduino outputs 0, 1, 2 and 3, which provide PWM signals when activated, to regulate the direction and speed of rotation.
- The Solid State Relay is powered from pin 4 of the Arduino and controls the power supply to the solenoid which is activated when it touches the ground surface to release the parachute.
- The Nicla Sense ME and GDK-101 sensors, ~~is~~ are connected to the Arduino via the I2C protocol.
- The Ultimate GPS module connects serially to the TX and RX pins.
- The thermal camera is connected to I2C
- The buzzer module is powered by the Arduino board to pin 6.
- The SD card module is the MKR Mem Shield, connected via the SPI protocol.
- The power source is a 4000mAh LiPo battery and supplies the system via a universal switch.

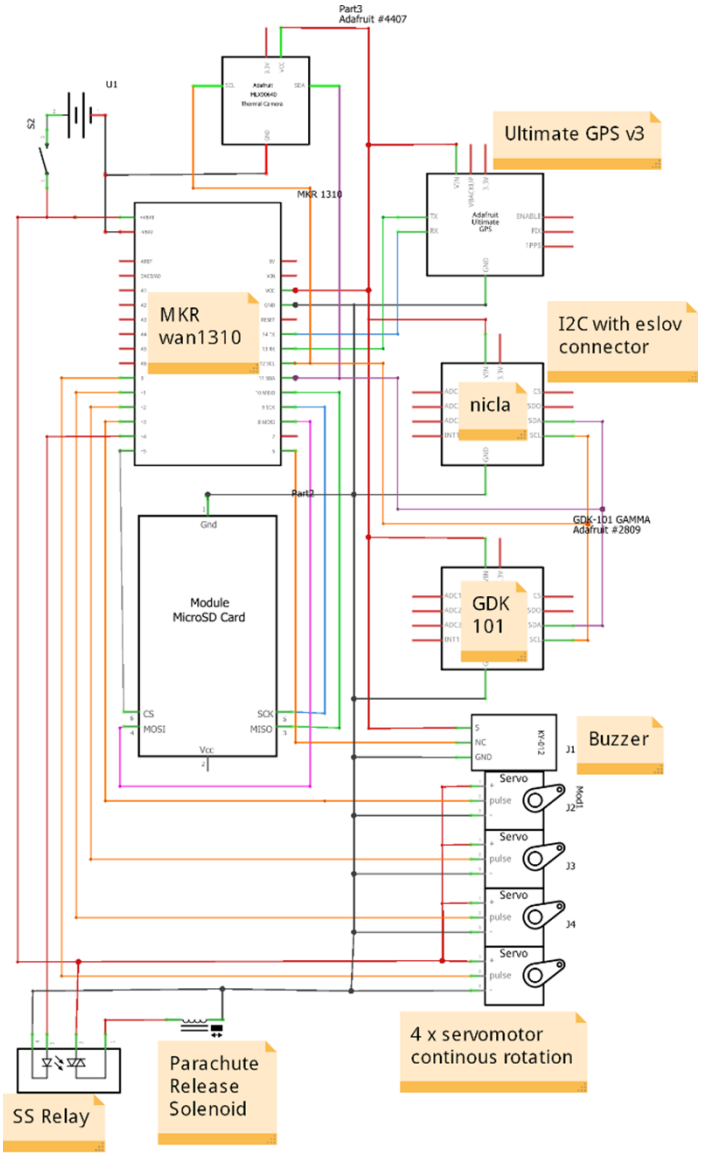

Figure 5. Electrical Wiring

Table 3. Required FRSR RU electrical components.

Component	Type	Im (mA)
LoRa Antenna	Microstrip LoRa Antenna	---
GPS Antenna	Antenna GPS	---
Battery	LiPoly Battery (4000mAh)	---
Arduino Board	MKR WAN 1310	0.1-140 max
Nicla Board	Nicla Sense ME	75 max
GPS	Adafruit Ultimate GPS v3	25 max
Solenoid	ZHO-0420L/S	400 max
Servo motor x4	FS90R CR	130-800 max
SD card module	MKR Mem Shield	4

Solid State Relay	FR120N	6
USB charger	MCP73831	-
Buzzer	Passive Buzzer Module	3
γ-radiation sensor	GDK101 sensor	20
Thermal camera	MLX90640	25
Main switch	SPST Switch	--

Data transmission will be held using the LoRa transmission protocol with the following characteristics for BS and RU (Table 4).

Table 4. Telecommunications setup

Parameter	**Value**
Communication scheme	LoRa
Frequency (f)	868MHz (EU zone)
Transmission Power (Pt)	25mW
Minimum receiving power (Pr)	-148dbm (1,6 10^{-15}mW)
Transmission data rate (r)	5Kbps

Energy Budget

For the calculation of the required energy, the worst possible scenario is considered, including a 10-minute flight to the disaster area. Theoretically, the maximum energy needs of the RU during flight will be:

$$E_{air} = \frac{t\,V\,\sum I_m}{L_h} \qquad Eq.1$$

Table 3 shows the sum of the current I_m consumed by all devices, except buzzer, solenoid and servo motors, is I_m=303 mA. All devices are supplied with voltage V=3.3 V. The maximum duration t of the flying mission operation (once activated) is maximum 10 min (t=600 s), while the energy loss factor is defined as L_h = 0.95.

From the above equation it follows that the required energy is E_{air} = 632 J for the 600s of flying time, so the system at the airborne phase will consume P_{air} = 1.05 W.

When the RU lands, the solenoid will be activated instantaneously, for about 1s, the solenoid will consume I_s=400 mA and the corresponding relay I_{ssr}=6 mA, so it will consume $E_{landing}$=1.3 J according to Eq.2:

$$E_{landing} = t\,V\,(I_s + I_{ssr}) \qquad Eq.2$$

After landing, the motors will start working, consuming an average of 400 mA each, i.e., 1.6 A altogether. So the power of the drive system on the ground will be $P_{mov} = 4\ I_{servo}\ V = 5.92$ *W, w*hile, the 4000 mAh battery has stored energy, E_{Bat} = *4000mAh x 3.7V = 14.8 Wh or 53.28 kJ.*

Therefore, with the drive system and data transmission activated, after landing, the RU will operate for 7092 s, or 1 h, 58 min and 13 s according to Eq.3, consuming the 80% of the battery's energy.

$$t = \frac{0{,}8\,E_{bat} - E_{air} - E_{landing}}{P_{air} + P_{mov}} \qquad Eq.3$$

Software

The coding functions of the FRSR at the RU are:

- the connection to the base station
- the acquisition of the measurements from the sensors and the images from the thermal camera
- the normalization of the values, i.e. convert them into unit values of the measured quantity
- the transmission to the base station
- the storage on the SD card
- the detection of whether the RU is on the ground, established by the accelerometer, which, at the time of the fall, will take values greater than 3 g.
- the parachute release when it reaches the ground
- the activation of the drive system
- the movement of the vehicle in a direction chosen by stochastic procedures or by the mission handler

Code Flow Diagram

The software presented at the Fig. 6 includes the scenario that the Rover's descent from altitude, use of the parachute and its release mechanism when it lands.

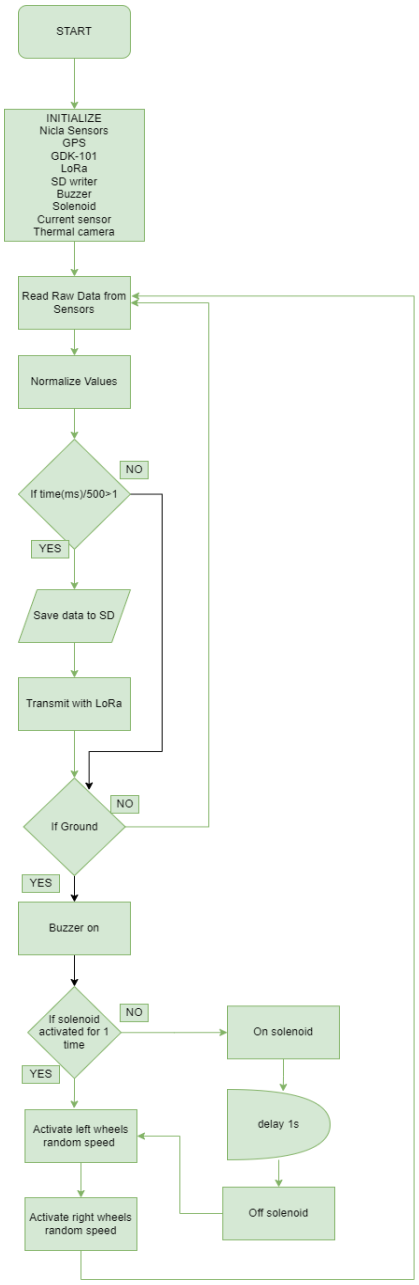

Figure 6. FRSR RU Coding Flow Chart

Thus, after the initialization of all individual systems, the values are read by the central unit and are normalized, every 1 s the current values are saved to the SD card and sent to the base station. If it is in the air, it continues to send values every second.

When it touches the ground, the microcontroller activates the solenoid only once to release the parachute. Next, the drive system is activated, which is different for the left and right sides and gives a random speed value on both sides allowing it to turn randomly ~~to~~ and explore the space.

Depending on the mission, the program can be extended so that the Rover approaches a specific point determined by the GPS coordinates.

Data Budget

Each transmission consists of the measurements of the 10 sensors and the GPS (2 values, latitude and longitude), which are transmitted. So, there are N_V=12 variables, where the data they produce will be stored and transmitted, with a frequency of f=1 Hz (1 measurement per second).

The image from the thermal camera has a resolution of 24x32 pixels and has a color depth of 4 bit, so the data produced by each image are D_{th}=384 bytes.

Therefore, the total data D, if each variable is of type "long" with d=4 Byte, for 2 hours (t=7200 s) of operation, will be:

$$D = (N_V\ d + D_{th})\ f\ t \qquad Eq.4$$

That is, D=11 750 400 Bytes or about 12MB.

The minimum necessary transmission rate R of the data (in bit/s) shall be:

$$R = (N_V\ d + D_{th})\ f\ 8 \qquad Eq.5$$

That is R=3456 bps, less than the maximum bit rate supported by LoRa systems which is R_{LoRa}=5 Kbps. So, the storage drive, the SD card, and the transmission system, LoRa, can easily handle the data amount that the FRSR requires.

Landing System

For the successful execution of the mission, a descent speed of 5 m/s was selected, ensuring a smooth landing and enough flight time to measure air quality during descent and to detect the change in values as it approaches the site of interest. The parachute characteristics will be:

Descent speed u=8 m/s
Coefficient C_d=1.25
Air density ρ=1.22 kg/m^3
Rover mass m=0.35 kg
Gravity acceleration g=9.81 m/s^2
The following formula (Eq.6) is using to calculate the parachute area:

$$A = \frac{2mg}{\rho C_d u^2} \qquad Eq.6$$

So, the parachute surface is A = 0,1836 m^2. To achieve this surface (Fig.7) we choose a base diameter D=0.5 m, upper opening diameter d=0.15 m. Eight equal sections were created ~~according to the~~ as shown in Figure 7 and the materials of the parachute are:

- Low weight fabric 27 g/m^2 ripstop type.
- The parachute mooring ropes are made of Kevlar material with a diameter of 0.8 mm, tensile strength of 62 kg and length L=1.15*D=0.575 m
- The ropes are fastened to the body of the Rover with a 20 kg swivel type coupling.

The estimated descent time from the maximum altitude h=200 m with speed u=5 m/s, will be
$t = \frac{h}{u} = \frac{200}{5} = 40$ s

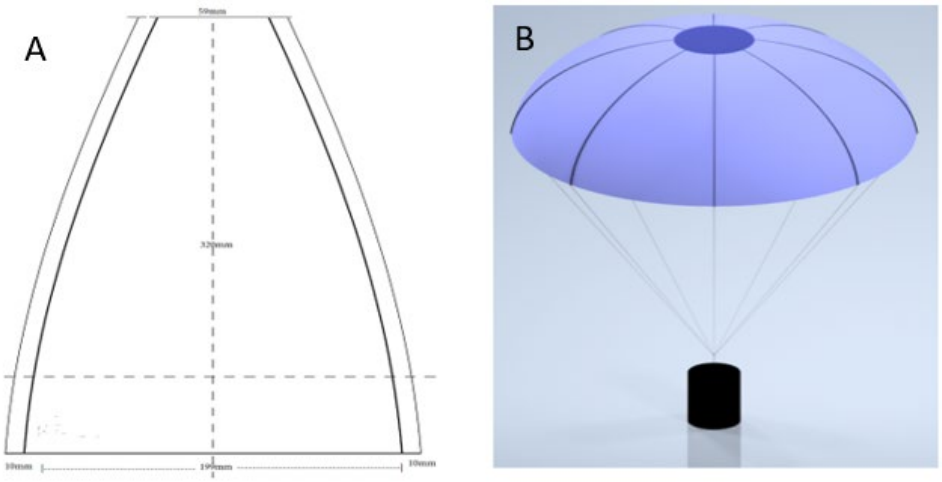

Figure 7. A. Parachute Drawing of 1 segment and B. 3-Dimensional Parachute Display

Base Station Equipment (BS)

The BS equipment includes a PC with a LoRa transceiver. It is possible to connect the BS to an Android smartphone with a USB connection cable and an OTG device. However, this BS setup increases the complexity, reduces the data processing capabilities and is beyond the scope of this work. We chose a simpler and more robust BS setup that includes a LoRa equipped Arduino connected to a laptop and a charged UPS in case if the operation needs more time to conclude. The required devices are described in the table 5 below.

Table 5. BS Equipment

Equipment	Description
laptop	PC Windows, 2 USB ports
LoRa module	Arduino MKR WAN 1300, 868 MHz, 25 mW, -148 dbm
Antenna	Microstrip

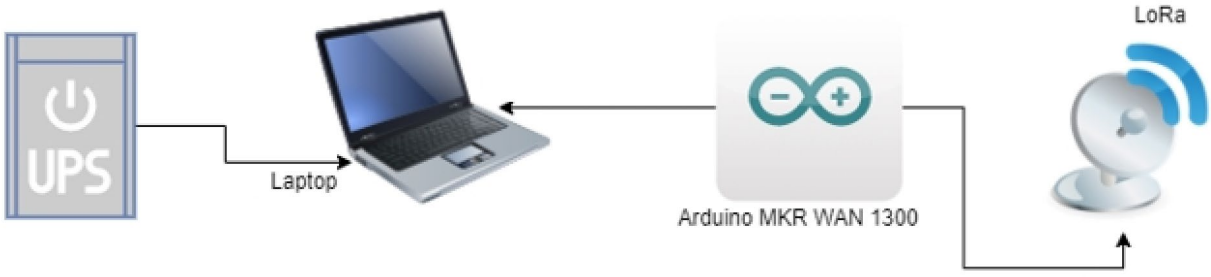

Figure 8. Base Station

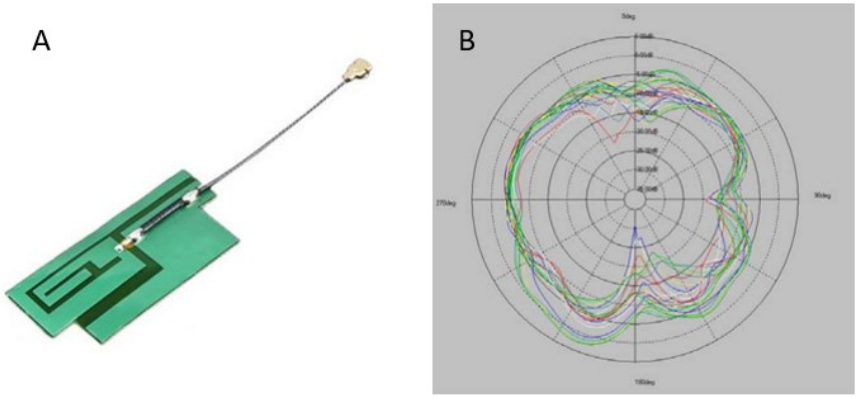

Figure 9. A. Microstrip antennas at BS and RU and B. Radiation Pattern

The antenna chosen for the BS and the RU is of the microstrip type [10], as this type takes up minimal space and does not create space management problems. The radiation pattern of the antenna is satisfactory, as it transmits almost omnidirectionally.

The data are stored on the hard drive of the PC in a .csv file through the Putty software. The data from the file will then be used to produce figures and warnings for possible hazardous conditions in the area. The software flow chart for the Arduino in the BS is presented in Figure 10.

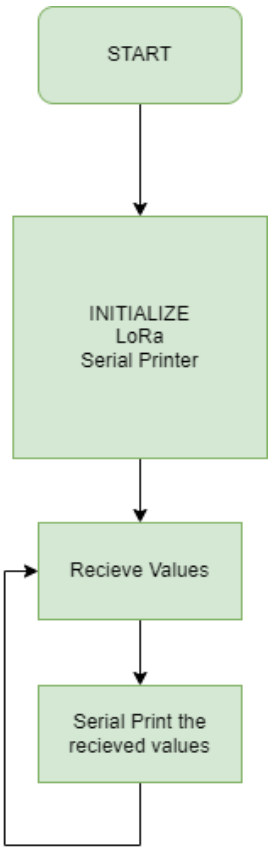

Figure 10. Coding Flow Chart for the Base Station

Estimated Cost

A major goal of this proposal is to keep the FRSR system cost low, so that it can be easily accessible to every rescue team. Thus, an effort is made to keep the total cost below 400 euros without reducing the quality of construction. Acquisition costs have been found to be a barrier to the availability and use of equipment. The table below breaks down the cost of the Rover.

Table 6. RU Cost Analysis

Component	**Quantity**	**Cost per Unit (€)**	**Total (€)**
LoRa antenna	1	2.90	2.90
GPS antenna	1	3.95	3.95
Battery	1	19.27	19.27
USB charger	1	5.89	5.89
Buzzer module	1	1.21	1.21
Thermal Camera	1	56.00	56.00
Utimate GPS v3	1	39.60	39.60
Arduino MKR MEM Shield	1	17.66	17.66
mSD 32GB	1	9.60	9.60
microServo SG90 cr	4	4.76	19.04
Solenoid	1	7.20	7.20
Nicla Sense ME	1	90.00	90.00
Arduino board MKR WAN 1310	1	36.21	36.21
γ-radiation sensor GDK-101	1	79.00	79.00
General Switch	1	5.00	0.16
Total cost			**390.59 €**

Results and Discussion

The testing procedures of the FRSR system were meticulously designed to simulate extreme and rapidly changing conditions, thus closely mirroring the real-world environments in which the system is expected to operate. To test the durability of the landing system and the ability to transmit data at high speeds, we tested the RU under extreme conditions, using a parachute with a descent speed of 8 m/s and deployed the FRSR's RU device from a high altitude, over 1300 m above ground level using a helicopter. This rigorous high-altitude drop test was conducted to assess the system's transmitting abilities during high-speed movement, as well as its responsiveness and accuracy in conveying real-time environmental data. Prior to the drop test, atmospheric conditions were extensively measured and recorded, providing a well-established baseline against which the data transmitted by FRSR-RU could be compared.

As the device descended at high velocity, its embedded sensors continuously measured variables such as the Air Quality Index (AQI), the presence of hazardous gases, the concentrations of Volatile Organic Compounds (VOC), the γ-radiation levels, the temperature, the humidity, the atmospheric pressure, and the geographical coordinates. The data were transmitted wirelessly to the BS, allowing for immediate comparison with the known atmospheric conditions. Throughout the descent, particular attention was given to any latency, noise, or error in the transmitted data, to assess the system's resilience and precision under extreme and variable conditions.

The collected data were subsequently utilized to produce a comprehensive set of graphs, further elucidating the system's performance under the simulated conditions.

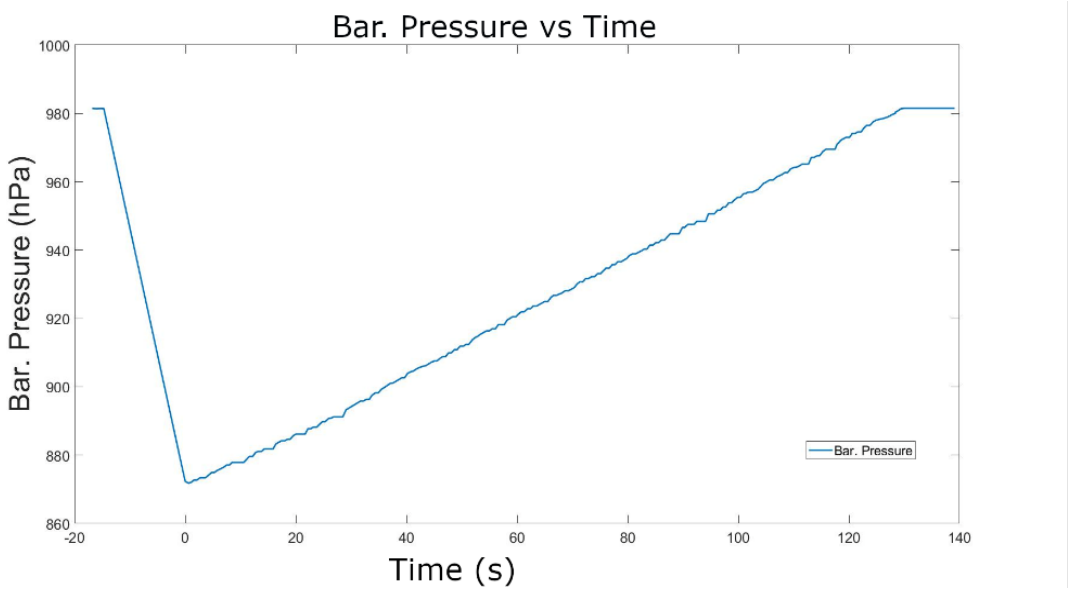

Figure 11. Atmospheric Pressure over Time, the atmospheric pressure sensor can be used for the altitude calculation. Figure 11 presents the pressure over time. As the pressure can be used to calculate the altitude of the RU the graph represents that the parachute works as it was designed to do, the altitude change is linear, corresponding to a constant RU descent speed of 8,3 m/s.

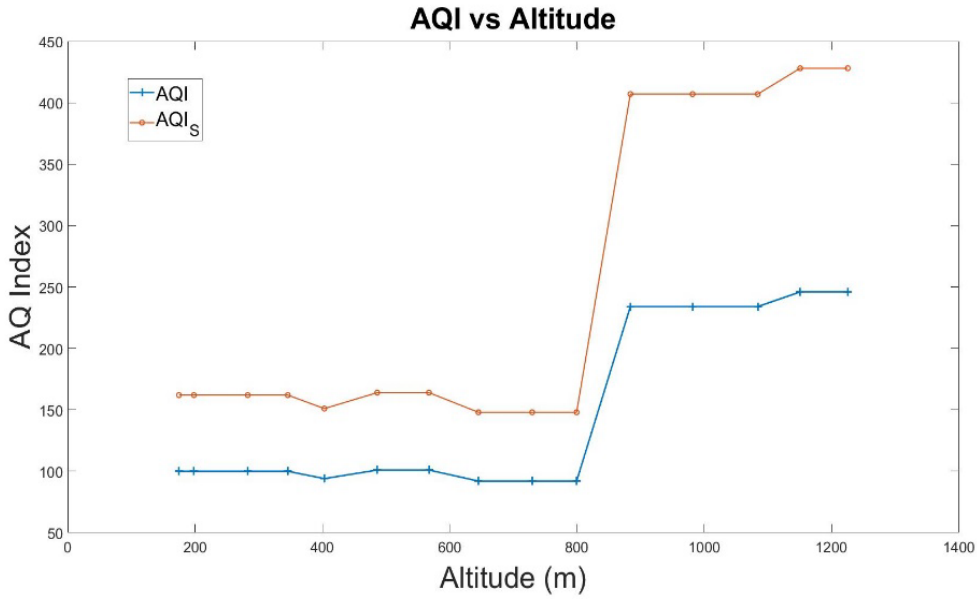

Figure 12. AQI over Altitude (see table 2)

Concerning the Air Quality Index (AQI) as shown in Figure 12, the sensor, augmented by AI technology, successfully recorded instantaneous AQI values. Notably, higher readings were registered at the peak altitude,

originating from the exhaust gases of the helicopter's engine. Subsequent readings aligned with the current values of the region as reflected on websites such as iqair.com [11] and meteo.gr [12] of the National Observatory.

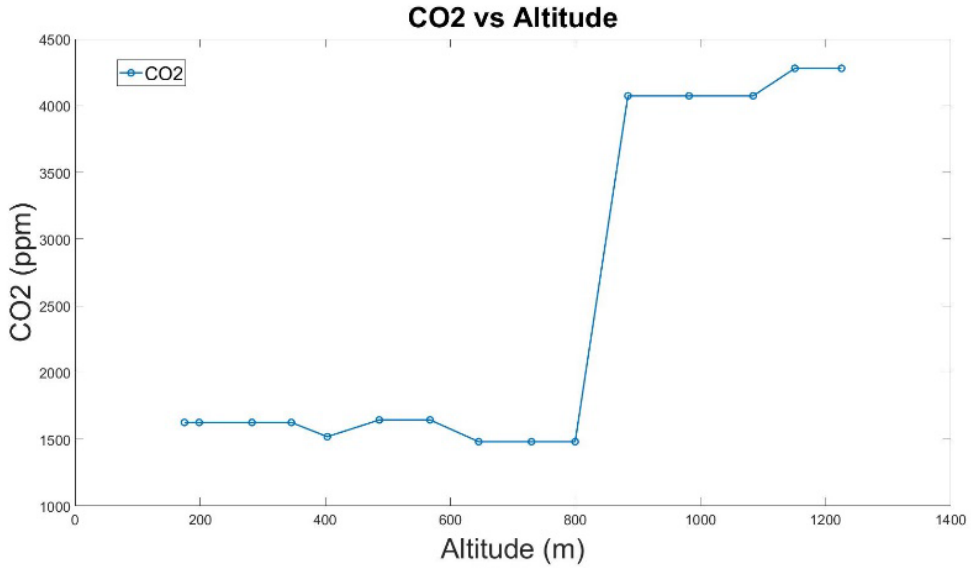

Figure 13. CO2 over Altitude

Similarly to the AQI graph, elevated levels of CO_2 near the peak altitude were discerned in the subsequent Figure 13, also attributable to the exhaust gases. At lower altitudes, the readings coincided with prevailing values in the region as per the local measuring stations [13].

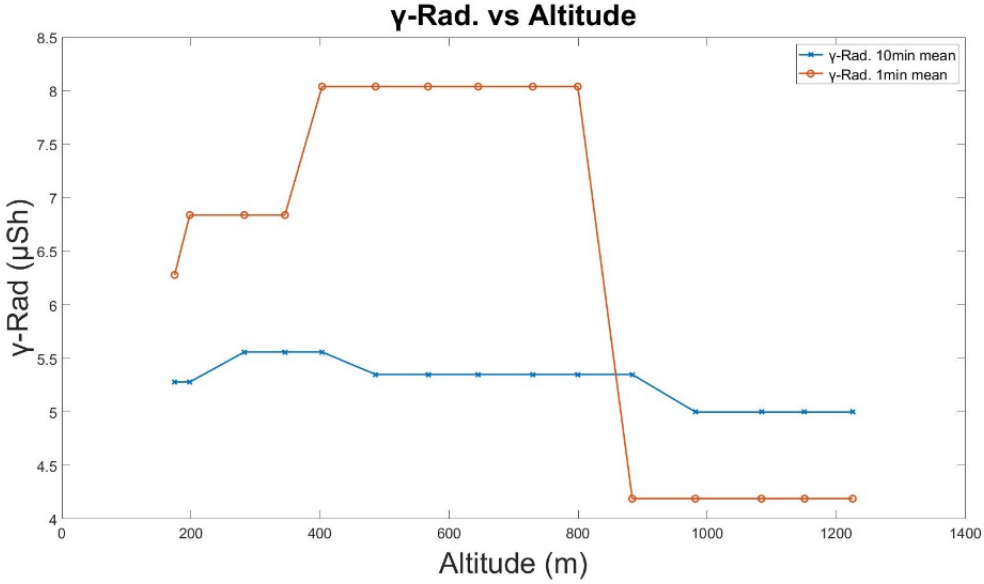

Figure 14. γ-radiation mean value of 10 minutes and 1 minute over Altitude

Figure 14 revealed nearly consistent radiation levels, with a slight increase at lower altitudes due to natural radiation emanating from ground materials. The one-minute average value logically presented this fluctuation more

prominently, with levels corresponding to those at the nearest measurement station of the Greek Atomic Energy Commission in Salamina [14].

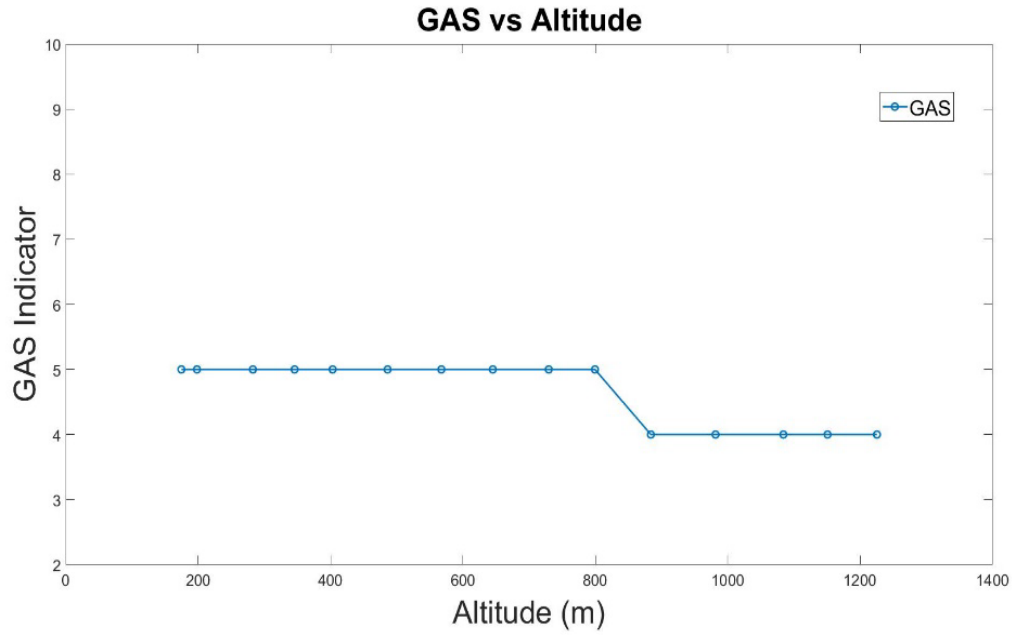

Figure 15. GAS indicator over Altitude (see table 2)

Minor variations were observed in the GAS index (Fig. 15) as lower altitudes showed a slight increase in pollution particles as expected.

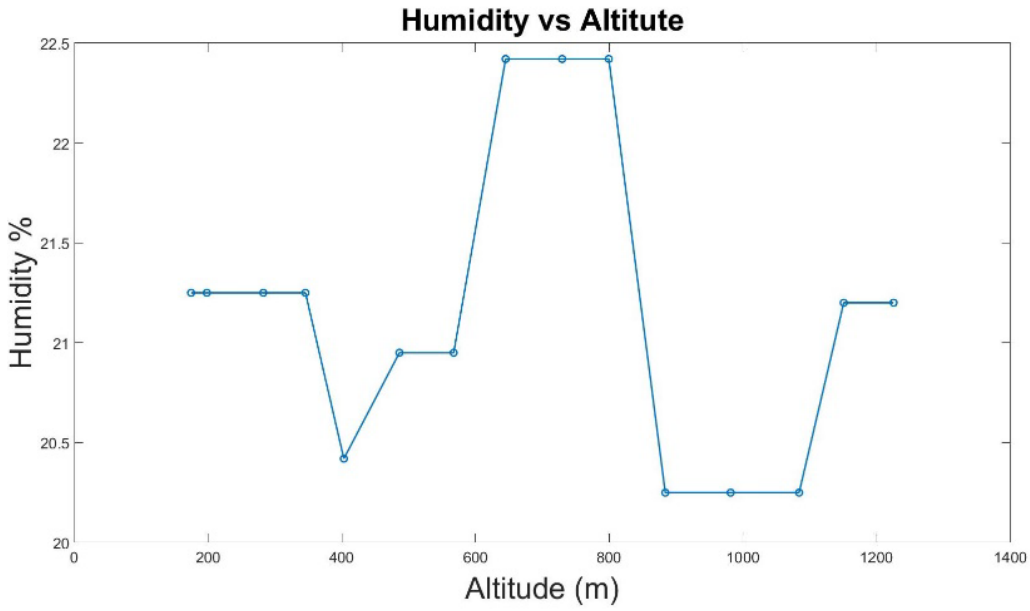

Figure 16. Atmospheric Humidity over Altitude

Humidity levels (Fig. 16) exhibited an elevation at mid-altitudes (600-800 m), likely due to the presence of

clouds at this specific height. Otherwise, the readings were consistent with those from the nearest ground station and followed the anticipated variation during descent.

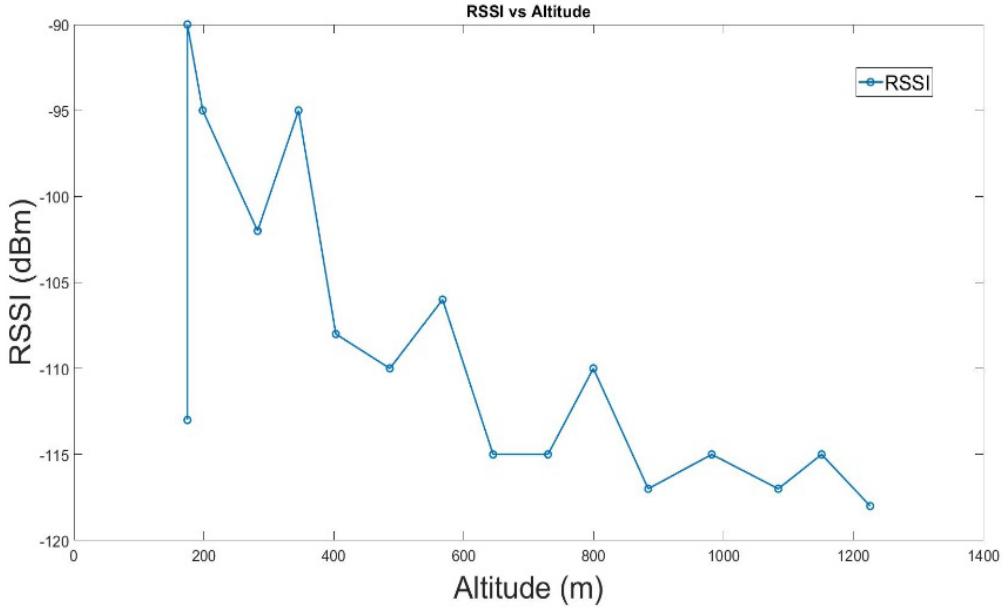

Figure 17. Received Signal Strength of the received signal at the BS over Altitude

The Received Signal Strength, as the RU descends is illustrated ~~at~~ in Figure 17. Despite the harsh conditions, distance and high descent speed, the received signal remained at levels well above the minimum operating limits of LoRa (less than -130 dBm), thus proving the robustness of the data transmission system in extreme conditions.

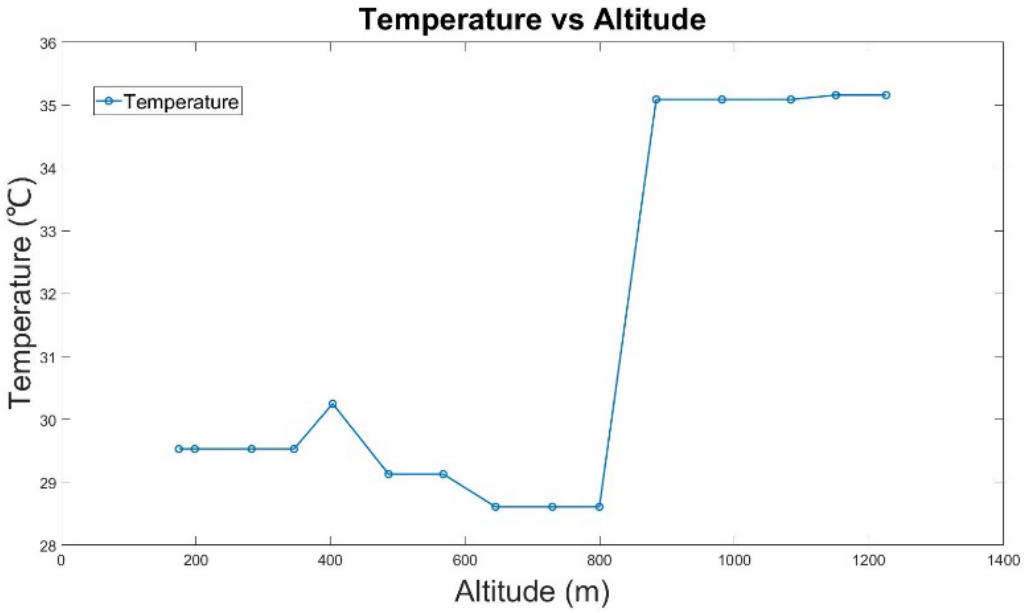

Figure 18. Temperature over Altitude

High-altitude temperatures are generally expected to be lower, however, the diagram (Fig. 18) shows elevated temperatures above 900 m. This anomaly was likely due to the flying device (helicopter) being exposed to the hot exhaust gases of the engine during its release.

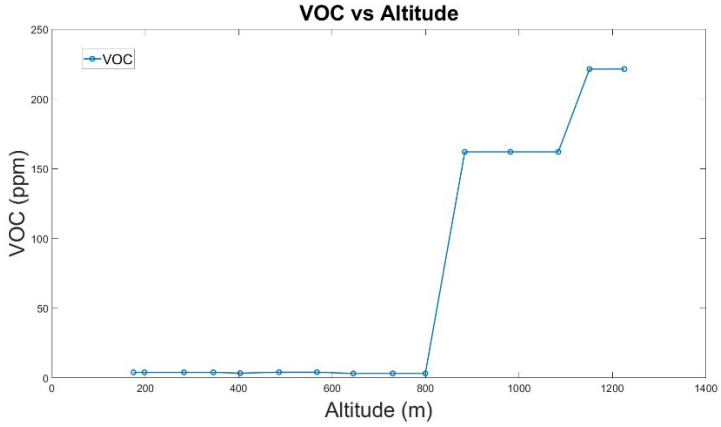

Figure 19. Volatile Organic Compound over Altitude

A similar phenomenon was observed in the following diagram (Figure 19), where the Volatile Organic Compounds (VOC) index exhibited high values at greater altitudes. This occurrence could be attributed to the presence of organic substances in the fuel used by the helicopter's propulsion system.

Overall, these findings contribute significantly to enhance our understanding of atmospheric variations with altitude and provide insights into the impact of human-made factors. The data serves as a valuable scientific resource for environmental monitoring, illuminating the complex interplay of various atmospheric parameters. Notably, the data closely aligns with measurements from nearby stations, confirming its reliability. The RU demonstrated its capability to detect rapid and abrupt changes in atmospheric conditions while moving at high speed. It also successfully identified emissions from the vehicle transporting it to ~~this~~ altitude. Throughout the mission, the RU transmitted all data seamlessly without issues. Upon reaching the landing site, the parachute, which ~~was~~ had already deployed, was detached from the device, allowing the RU to begin exploring the area using its mobility system, while continuing to transmit data without interruption.

Conclusion

In this study, we propose and extensively test the FRSR system, which comprises a Rover Unit and a Base Station The system demonstrates exceptional performance and reliability while maintaining ~~at~~ a significantly low cost. With a total cost under 400 euros and no need for specialized base stations, the device stands out as an economically viable option. This affordability, coupled with its robust functionality, makes it particularly accessible to a wide range of users, including rescue teams operating in diverse environments.

The device's efficient communication system achieved a 99% operation rate with minimal packet loss, even when encased in a protective housing that functioned as a Faraday cage. This performance was coupled with a precise parachute design allowing a controlled landing within 20 meters of the launch site, facilitating easy recovery. The choice of a simple microstrip antenna ensured successful communication over distances up to 1000 meters, proving that expensive and complex systems are unnecessary for effective data transmission in this context. The robust mechanical design ensured all components remained intact through the stresses of launch and landing.

Further, the device continued to operate effectively for 13 hours after landing, even without utilizing the drive system, demonstrating its suitability for extended missions. It successfully measured and transmitted crucial

environmental parameters including AQI, VOCs, various gases, humidity, pressure, and radioactivity. This performance highlights the effectiveness of its integrated sensors.

Overall, this mission demonstrated not only the technological reliability and scientific value of the device but also its economic efficiency. With a low cost and operational simplicity, the device proves to be a practical tool for various applications-especially for rescue teams operating under budget constraints and in challenging environments. The low cost and operational simplicity of the device make it an accessible and valuable resource for environmental monitoring and emergency operations worldwide.

Acknowledgments

I would like to thank my advisor for the valuable insight provided to me on this topic.

References

[1] Cheng, Wan-Li, et al. "Comparison of the revised air quality index with the PSI and AQI indices." Science of the Total Environment 382.2-3 (2007): 191-198.
[2] Fitz-Simons, T. Guideline for reporting of daily air quality: Air Quality Index (AQI). No. PB-99-169237/XAB; EPA-454/R-99/010. Environmental Protection Agency, Office of Air Quality Planning and Standards, Research Triangle Park, NC (United States), 1999.
[3] Neubert, Sebastian, et al. "Flexible IoT Gas Sensor Node for Automated Life Science Environments Using Stationary and Mobile Robots." Sensors 21.21 (2021): 7347.
[4] Dueker, Heinrich, Karl-Hermann Friese, and Wolf-Dieter Haecker. "Ceramic aspects of the bosch lambda-sensor." SAE Transactions (1975): 807-824.
[5] Ghebretinsae, F., O. Mikkelsen, and A. D. Akessa. "Strength analysis of 3D printed carbon fibre reinforced thermoplastic using experimental and numerical methods." IOP conference series: materials science and engineering. Vol. 700. No. 1. IOP Publishing, 2019.
[6] Nakagawa, Yuki, Ken-ichiro Mori, and Tomoyoshi Maeno. "3D printing of carbon fibre-reinforced plastic parts." The International Journal of Advanced Manufacturing Technology 91.5 (2017): 2811-2817.
[7] Chen, Yuan, and Lin Ye. "Topological design for 3D-printing of carbon fibre reinforced composite structural parts." Composites Science and Technology 204 (2021): 108644.
[8] Chilingarian, A., et al. "Origin of enhanced gamma radiation in thunderclouds." Physical review research 1.3 (2019): 033167.
[9] Pound, Robert V., and Joseph L. Snider. "Effect of gravity on gamma radiation." Physical Review 140.3B (1965): B788.
[10] Adrovic, Feriz, ed. Gamma radiation. BoD–Books on Demand, 2012.
[11] Air quality in Megara, Air quality index (AQI) and PM2.5 air pollution in Megara, https://www.iqair.com/greece/attica/megara
[12] Meteo.gr, Greek National Observatory, Air Quality at Megara Attica, https://www.meteo.gr/cf-aqi.cfm?city_id=213
[13] Geodata.gov.gr, Greek Ministry of Environment, Measurements at Elefsina Station, https://geodata.gov.gr/dataset/stathmoi-metreses-atmospharikes-rupanses
[14] γ-radiation levels, Greek Atomic Energy Commission, https://eeae.gr/επίπεδα-ραδιενέργειας-στο-περιβάλλον/μέτρηση-σταθμού
[15] Sun, Tony, et al. "Reliable sensor networks for planet exploration." Proceedings. 2005 IEEE Networking, Sensing and Control, 2005., IEEE, 2005.
[16] Troutman, Patrick A., et al. "Revolutionary concepts for human outer planet exploration (HOPE)." AIP

Conference Proceedings. Vol. 654. No. 1. American Institute of Physics, 2003.
[17] Squyres, Steven. Roving Mars: Spirit, Opportunity, and the exploration of the red planet. Hachette UK, 2005.